Population analysis and immunologic landscape of melanoma in people living with HIV

Lindsay N Barger[1,2,3], Derek Wang[4], Ashley L Saravia[3], Valeria Mezzano[5,6], Gyles Ward[6], Cynthia Loomis[5,6], Carly Feldman[7], Madalina Tuluc[8], Rino S Seedor[7,2], Peter J Gaskill[1,2], Anna E Coghill[9], Gita Suneja[10], Iman Dehzangi[4,11,12], Jennifer L Hope[3,2], George Jour[5,13], Gabriele Romano[1,2]*

[1]Department of Pharmacology and Physiology, Drexel University College of Medicine, Philadelphia, Pennsylvania.

[2]Immune Cell Regulation & Targeting Program, Sidney Kimmel Comprehensive Cancer Center, Philadelphia, Pennsylvania.

[3]Department of Microbiology and Immunology, Drexel University College of Medicine, Philadelphia, Pennsylvania.

[4]Center for Computational and Integrative Biology (CCIB), Rutgers University, Camden, New Jersey

[5]Department of Pathology, New York University Langone Medical Center, New York, New York

[6]Experimental Pathology, Division of Advanced Research Technologies, New York University Langone Medical Center, New York, New York.

[7]Department of Medical Oncology, Thomas Jefferson University Hospital, Philadelphia, Pennsylvania.

[8]Department of Pathology and Genomic Medicine, Jefferson University Hospital, Philadelphia, Pennsylvania.

[9]Cancer Epidemiology Program, Moffitt Cancer Center, Tampa, Florida

[10]Department of Radiation Oncology, Huntsman Cancer Institute, Salt Lake City, Utah

[11]Department of Computer Science, Rutgers University, Camden, New Jersey

[12]Rutgers Cancer Institute, Rutgers University, New Brunswick, New Jersey

[13]Department of Dermatology, New York University Langone Medical Center, New York, New York

***Correspondence:** Gabriele Romano – gr476@drexel.edu

Keywords: melanoma, HIV, T cells, MDSCs, immunotherapy, chronic infection

Funding: G.R. is supported by: WW Smith Charitable Trust - Medical Research Program (#C2303); Department of Defense - Congressionally Directed Medical Research Programs, Melanoma Research Program (ME220048); American Cancer Society (DBG-23-1036360-01); Comprehensive NeuroHIV Center (CNHC) Developmental Research and Mentoring Core (NIMH - P30MH092177); Sidney Kimmel Comprehensive Cancer Center (#00023568 and #901333). L.B. is supported by the Translational Research Training Grant in NeuroHIV (NIMH, T32-MH079785). P.J.G is supported by the National Institute of Drug Abuse, DA057337 and DA058051. Experimental Pathology Research Laboratory [RRID: SCR_017928] is partially supported by the Cancer Center Support Grant (P30CA016087). The original Akoya/PerkinElmer Vectra® multispectral imaging system was awarded through the Shared Instrumentation Grant S10 OD021747.

Acknowledgments: We thank the AIDS and Cancer Specimen Resource (ACSR) for providing tumor samples from PLWH; ACSR is funded by the National Cancer Institute.

Conflict of interest statement: The authors declare no conflicts of interest.

Abstract

Purpose: To dissect the clinical and immunological features of people living with HIV (PLWH) diagnosed with melanoma, who have consistently exhibited worse clinical outcomes than HIV-negative individuals (PLw/oH) with the same cancer. **Experimental Design:** We analyzed electronic health records from 1,019 PLWH and 373,121 PLw/oH diagnosed with melanoma. Demographic and clinical characteristics were compared. Spatial immune transcriptomics (72 immune-related genes) was performed on melanoma tumor samples (n=11), followed by downstream validation using multiplex immunofluorescence (n=15 PLWH, n=14 PLw/oH). **Results:** PLWH were diagnosed with melanoma at a younger age, had a higher representation of Hispanic and Black individuals compared to PLw/oH, and a decreased survival rate. PLWH also showed a markedly increased risk of brain metastases. PLWH experienced significant delays in initiating immune checkpoint inhibitor (ICI) therapy and had worse survival outcomes following ICI, even after balancing for demographic covariates. Spatial transcriptomics revealed a more immunosuppressive tumor microenvironment in PLWH, with upregulation of immune checkpoints (PD1, LAG3) and reduced expression of antigen presentation markers (HLA-DRB, B2M), with distinct spatial distributions in tumors and their microenvironments. Multiplex immunofluorescence confirmed an exhausted $CD8^+$ T cell compartment in PLWH, including enrichment of $PD1^{int}LAG3^-$ and $PD1^{int}LAG3^+$ subpopulations, and a significant accumulation of immunosuppressive myeloid-derived suppressor cells ($CD11b^+$ $HLA\text{-}DR^-$ $CD33^+$).

Conclusions: Our findings suggest chronic HIV infection fosters a permissive tumor microenvironment that might undermine effective immune responses and contribute to poor clinical outcomes for PLWH with melanoma. Targeting the actionable immune pathways identified in this study could inform tailored therapeutic strategies to mitigate these disparities.

Statement of translational relevance

This study reveals critical barriers to effective melanoma treatment in people living with HIV (PLWH). Despite receiving immune checkpoint inhibitors (ICIs), PLWH face delayed therapy initiation, a greater likelihood of brain metastases, and significantly higher long-term mortality—even after adjusting for demographic covariates. Transcriptional immune profiling further uncovers a tumor microenvironment enriched in immunosuppressive myeloid-derived suppressor cells and dysfunctional $CD8^+$ T cell populations with features of exhaustion. Together, these findings suggest that the inferior outcomes in PLWH are not solely due to delayed care but also reflect unique, targetable mechanisms of immune dysfunction. By defining the clinical and immunological features of this population, this work highlights opportunities for precision immunotherapy approaches tailored to PLWH with melanoma, with direct implications for improving survival and reducing disparities.

Introduction

Advancements in antiretroviral therapies (ART) have transformed HIV infection from a terminal diagnosis into a chronic condition, allowing people living with HIV (PLWH) to achieve a life expectancy nearly equal to that of the general population [1,2]. However, despite the success of ART in suppressing viral replication, HIV remains a lifelong infection due to its ability to integrate into host genomes and establish a state of latency, particularly within long-lived memory T cells and myeloid cells in sanctuary sites [3-5]. While ART prevents the spread of the infection, it does not eliminate pre-existing reservoirs that harbor integrated and latent viruses, leaving PLWH with persistent immune dysregulation and, therefore, increased susceptibility to age-related diseases [6]. Among these, non-AIDS-defining cancers (NADCs) have emerged as a major cause of mortality, including cutaneous melanoma [6]. Several reports on melanoma in PLWH point to disproportionately worse clinical outcomes compared to melanoma patients without HIV, despite adjustment for key factors such as disease stage at presentation [7-9]. The mechanisms underlying this disparity remain poorly understood. In particular, it is largely unknown how chronic HIV infection alters anti-tumor immune responses, which are particularly critical for melanoma, given the central role of the immune system in the progression and response to treatment in this type of malignancy.

To address this major knowledge gap, we first analyzed publicly available clinical datasets to compare demographics and outcomes between PLWH and HIV-negative individuals (PLw/oH), revealing significant disparities in demographics, metastasis risk, and survival after a melanoma diagnosis. We then performed the first immune-focused spatial transcriptomic analysis of melanoma tumors according to patient HIV status, uncovering striking differences in tumor-associated T cell and myeloid populations in PLWH. These findings were further validated and expanded using multiplex immunofluorescence to characterize immune cell phenotypes and subpopulations. Together, our data reveal a profoundly altered immune landscape in melanoma among PLWH, marked by T cell exhaustion and myeloid-mediated suppression, which underscores the need for tailored therapeutic strategies in this population with suboptimal clinical outcomes.

Results

PLWH with melanoma display increased overall mortality rates and brain metastasis risk.

To evaluate population differences between PLWH and PLw/oH diagnosed with melanoma, we interrogated the TriNetX US Collaborative Network dataset. Our study included two cohorts: 1,019 PLWH with melanoma and 373,121 melanoma patients without HIV. Baseline demographic analysis revealed that PLWH were diagnosed with melanoma at a younger age (58.5 ± 12.2 years in PLWH vs. 62.9 ± 15.6 years in PLw/oH) and were more likely to be male (80% vs. 52%, **Table 1**). Racial and ethnic distribution also differed between the cohorts. PLWH with melanoma exhibited a higher representation of Hispanic or Latino individuals (4% vs. 2%) and Black or African American individuals (7% vs. 1%) compared to their non-HIV counterparts (**Table 1**).

Ten-year survival rate (72.29% vs 77.22%, PLWH vs. PLw/oH, p=0.0076) was significantly lower in PLWH (**Fig. 1A**, **Table S1**), suggesting a worse long-term prognosis, consistent with previous reports [7]. The two cohorts had a similar median follow-up time of approximately 3.2 years (PLw/oH) and 4.2 years (PLWH, Table S2). Our analysis focused on patients diagnosed during the ART era (98.4% of patients had ART treatment records; patients diagnosed before 2005 were not available). Significantly different survival rates were detected even after balancing the cohorts for demographic covariates (72.29% vs 80.82% survival rate, PLWH vs. PLw/oH, p=0.00252, **Fig. 1B, Table S3-4**). Staging information and BRAF status were only available for <1% of the population, and no robust statistical assessment could be performed on these aspects. Nevertheless, given the impact of metastasis on cancer mortality, we assessed the risk of melanoma spreading to its most frequent metastatic sites. No significant differences were detected between the two groups of patients in terms of metastasis at presentation/early metastasis (0 days to 6 months after diagnosis, **Table S5**). Interestingly, while there were no significant differences in lung, liver, or lymph node metastases, PLWH had a significantly higher risk of late brain metastases (>6 months after diagnosis, p<0.0001, risk ratio = 1.98, **Table S5**), and an overall increased risk of metastatic disease in the long term (p<0.0001, risk ratio = 1.484, **Table S5**).

Next, we focused on FDA-approved immune checkpoint inhibitors (ICIs) to evaluate differences in treatment patterns and outcomes between the two groups. ICIs serve as the first-line treatment approach for patients with advanced melanoma, and analyzing their use provides insights into how patients with late-stage disease fare in the clinical setting. Among our cohorts, approximately 9% of PLWH (n=91) and 6% of PLw/oH (n=22,700) had a record of receiving immune checkpoint therapies. The demographic features of these two sub-groups reflected the differences we detected between the parent cohorts (**Table 2**). Although we were not statistically powered enough to draw conclusions for specific treatment regimens, we were able to make some comprehensive observations regarding ICI outcomes and timing. We found that, on average, PLWH experienced longer delays before initiating treatment compared to PLw/oH (p=0.0099, **Table 2**). This is consistent with existing knowledge that PLWH face barriers to timely treatment, possibly due to differences in healthcare access, treatment prioritization, or delays in clinical decision-making. In the PLWH cohort we did observe a significantly higher number of patients with lymph node metastasis at presentation (p=0.0005, **Table 2**). Once ICI was initiated, we did not detect differences in treatment duration (**Table 2**). We then performed a ten-year survival analysis of the two cohorts. PLWH demonstrated significantly lower probabilities of survival compared to the non-HIV melanoma patients (10-year, 20.77% vs 47.12% survival rate, PLWH vs. PLw/oH, p=0.036, **Fig. 1C**, and **Table S6**). Such significant differences persisted even after adjusting for demographic covariates, and metastasis at presentation (10-year, 31.26% vs 59.36% survival rate, PLWH vs. PLw/oH, p=0.0296, **Fig. 1D**, and **Table S7-8)**

PLWH display an immunosuppressive and exhausted melanoma tumor microenvironment

143 Our data indicate that PLWH who develop melanoma experience an overall elevated mortality rate,
144 also in the sub-cohort who received ICI. While demographic differences, higher rates of coexisting conditions,
145 and psychosocial barriers are contributors to mortality, the decreased survival rate persisted even after
146 balancing cohorts for demographic covariates and metastasis occurrence, indicating there may also be
147 underlying biological or immunological components. To explore this, we collected tumor samples from 11
148 PLWH with melanoma and matched them with samples from 11 patients without HIV (PLw/oH) with
149 melanoma with similar clinical and demographic features (**Table S9)**.

150 For each sample, we processed three to five regions of interest (ROIs) for spatial immune
151 transcriptomics (72 immune-related genes). A pathologist selected the ROIs based on morphology and the
152 expression of melanocytic markers, labeling subregions as either "tumor-cell rich" (TUMOR) or "tumor-
153 microenvironment rich" (TME, **Fig. S1**). To identify differences in gene expression between PLWH and
154 PLw/oH, we performed differential expression analysis (DEGs) using the DEseq2 algorithm, comparing the
155 TME and TUMOR regions. The analysis revealed significant gene expression differences between the
156 groups, suggesting distinct immunological characteristics associated with HIV status (**Fig. 2**).

157 When comparing the TME and TUMOR areas of PLWH with PLw/oH, we observed increased
158 expression of several immune checkpoint genes, including *PD1*, *LAG3*, *CTLA4*, *TIGIT*, *CD276,* and *ICOSLG*.
159 Notably, *LAG3* emerged as the top-scoring immune checkpoint in the TUMOR, while *PD1* was the highest in
160 the TME (**Fig. 2A- B**). This suggests that there are distinct spatial distributions of varying T cell populations
161 within these tumors. Both the TUMOR and TME exhibited additional characteristics of an immune-
162 suppressive or evasive microenvironment. In the TUMOR compartment, we observed elevated expression
163 of *IDO1*, a key protein that inhibits T-cell function (**Fig. 2A**). Meanwhile, the TME showed reduced expression
164 of *HLA-DRB* and *B2M,* which are MHC class II and I molecules essential for antigen presentation (**Fig. 2B**).
165 Several key genes involved in immune responses were also downregulated, including *IFNGR1*, *CD74*, *LY6E*,
166 and *STAT2*. Beyond immune regulation, we identified an interesting pattern of differential gene expression
167 pertaining to fibrosis and extracellular matrix (ECM) remodeling in the TME. PLWH demonstrated a decline
168 in the expression of *CD44*, *ITGAV*, *and PECAM1* and increased *ITGB8*, suggesting alterations in tumor-
169 stroma interactions that may contribute to disease progression (**Fig. 2B**).

170 Interestingly, a small cadre of genes associated with enhanced inflammation was identified in the
171 TME of PLWH, including an increase in *IL-15*, *TBX21*, and *CCL5* (**Fig. 2B**). In the TUMOR, there was an
172 increase in *BATF3*, which is mostly expressed on $CD8^+$ cells (i.e., dendritic cells and T cells) (**Fig. 2A**).

173 To summarize our findings and prioritize downstream validation, we ran a modified version of the
174 MCPcounter algorithm, utilizing tailored gene sets that included population marker genes and immune
175 signaling genes (**Table S10-12**). The only two upregulated gene sets in PLWH, both in TME and TUMOR
176 areas, were immune checkpoints and myeloid suppressive signaling (**Fig. 2C**). In terms of immune
177 populations, overall, it appeared that the TUMOR areas from PLWH were generally enriched in immune cells
178 both from myeloid and lymphoid origin, and displayed enhanced expression of several immune signaling

179 pathways (**Fig. 2C and Fig. S1**). The TME areas were, in general, more similar between PLWH and PLw/oH
180 (**Fig. S2**).
181
182 **PLWH display distinct subsets of CD8$^+$ T cells within the melanoma tumor environment**
183 To validate and further expand upon the spatial transcriptomics findings, we investigated T cell
184 populations using multiplexed immunofluorescence staining (mIF). The cohort included melanoma tumor
185 samples from 15 HIV$^+$ and 14 HIV$^-$ patient samples, with 11 samples in each group overlapping with those
186 profiled by spatial transcriptomics. We examined T cell populations within both the tumor bulk and peripheral
187 edges using an mIF panel targeting T cell populations (CD8, CD4, Foxp3), along with the two top-scoring
188 immune checkpoint inhibitors identified in our transcriptional analysis (LAG3 and PD1) (**Fig 3A**). While
189 melanocytic markers were excluded from this panel, a pathologist histologically assessed the sections to
190 delineate tumor regions and guided the analysis. Thus, the results reflect the tumor specimens as a whole
191 instead of the specific delineation of sub-regions.
192 Analysis of the T cell compartment revealed no significant differences in the overall frequency of CD8$^+$
193 or CD4$^+$ T cells between melanoma tumors in PLWH and uninfected patients (**Fig. 3B-C**). Similarly, regulatory
194 T cells (T_{REG}, CD4$^+$FOXP3$^+$) abundance did not differ significantly between groups (**Fig. S3A**). Notably, PLWH
195 exhibited altered T cell proportions, with a significantly reduced CD4$^+$:CD8$^+$ ratio and a lower Foxp3$^+$:CD8$^+$
196 ratio, suggesting a shift in the relative balance of T cell subsets (**Fig. 3D-E**).
197 We next interrogated the co-expression of immune checkpoint receptors PD1 and LAG3 on CD4$^+$
198 and CD8$^+$ T cells. PD1 expression was stratified into three tiers (PD1$^-$, PD1^{int}, and PD1^{high}), and LAG3 into
199 two (LAG3$^-$ and LAG3$^+$), based on previous reports highlighting functional differences in cytotoxicity and
200 exhaustion in these subpopulations [10-12]. No significant differences were observed in CD4$^+$ T cell subsets
201 between PLWH and PLw/oH (**Fig. S3B-E**).
202 Interestingly, we identified distinct subpopulations of CD8$^+$ T cells in PLWH compared PLw/oH.
203 Specifically, melanoma tumors from PLWH showed significant enrichment of the CD8$^+$PD1^{int} LAG3$^-$ and the
204 CD8$^+$PD1^{int} LAG3$^+$ populations (**Fig. 3F-G**). Notably, we did not detect any differences in the abundance of
205 PD1^{high} cells, whether they were LAG3$^+$ or LAG3$^-$ (**Fig. 3H-J**).
206 Given the important role of the myeloid compartment in modulating T cell function, we next turned our
207 focus to tumor-associated myeloid populations.
208
209 **PLWH exhibit an enriched population of immunosuppressive myeloid cells in melanoma**
210 **tumors**
211 Pathway analysis highlighted myeloid suppressive signaling as a top candidate (**Fig. 2C**) and a
212 significant downregulation of key components of antigen presentation, such as *HLA-DRB*, within the tumor
213 regions (**Fig. 2**). In parallel, previous studies have reported that PLWH have elevated levels of myeloid-
214 derived suppressor cells (MDSCs) at baseline, a population of highly immunosuppressive, immature myeloid

215 cells [13,14]. Based on these findings, we selected CD11b to broadly define the myeloid lineage and included
216 HLA-DR, CD33, and CD66b to resolve functional subpopulations, including potential MDSCs. Using
217 multiplexed immunofluorescence (mIF) on the tumor samples previously analyzed for T cell populations, we
218 identified a significant increase in CD11b$^+$ HLA-DR$^-$ myeloid cells in PLWH (**Fig. 4B**), consistent with an
219 immature or non-antigen-presenting phenotype. Most of these cells also expressed CD33, supporting their
220 classification as monocytic-like MDSCs (M-MDSCs) (**Fig. 4C**). In contrast, no differences were observed in
221 CD11b$^+$ HLA-DR$^-$ CD66b$^+$ cells, or polymorphonuclear-like MDSCs (PMN-MDSC) between PLWH and
222 PLw/oH (**Fig. 4D**) [15].
223

224 Discussion

225 The present study demonstrates that PLWH who develop melanoma experience distinct clinical
226 outcomes and tumor microenvironments compared to those without HIV. Notably, PLWH exhibited increased
227 overall mortality, including in the subpopulation of patients who underwent ICI. Such an increase persisted
228 also after balancing cohorts for demographic covariates. Immune-focused spatial transcriptomics analysis
229 suggested that melanoma in PLWH displayed an enhanced suppressive and exhausted tumor
230 microenvironment. Multiplex immunofluorescence further identified an enrichment of unique CD8$^+$ T cell
231 subsets, indicating a skewed T cell activation/exhaustion profile, alongside an increased presence of MDSCs,
232 which are known to inhibit T cell function and promote immune suppression.

233 Our results highlight the unique immunological features in melanoma tumors of PLWH, emphasizing
234 the need for updated targeted interventions. Despite the growing use of ICI in melanoma and several reports
235 demonstrating safety in PLWH [16], this patient population was largely excluded from oncology clinical trials,
236 resulting in a significant gap in reliable data regarding the efficacy of ICI use within this population [17,18]. This
237 exclusion fosters a cycle of provider hesitancy and continued research omission, ultimately limiting access
238 to optimal cancer care and contributing, in part, to increased melanoma mortality [17]. Consistent with these
239 challenges, our study demonstrates that PLWH experience significantly longer delays in treatment initiation
240 compared to individuals without HIV. This exacerbates disease progression and can contribute to the
241 increased melanoma mortality rate in PLWH that we report here. This delay likely stems from both the clinical
242 uncertainty due to the lack of clinical trial data and psychosocial barriers, including healthcare access
243 disparities and medical mistrust linked to historical HIV-related stigma, as we have previously reviewed [19].
244 Addressing these barriers is critical to improving melanoma outcomes for PLWH.

245 Additionally, our findings indicate a significantly higher risk of metastasis in the long term in PLWH,
246 especially brain metastasis, suggesting a potential immune surveillance vulnerability that facilitates
247 melanoma dissemination and/or outgrowth to the brain. HIV infiltrates the brain early in the infection,
248 contributing to chronic neuroinflammation and the development of HIV-associated neurocognitive disorder
249 (HAND) [20]. This disruption of the blood-brain-barrier may create a permissive environment for melanoma
250 cells to colonize there [21]. This increased risk highlights the importance of heightened cancer surveillance and

early treatment strategies for this population, as literature shows that the occurrence of brain metastasis significantly lowers the probability of survival and response to therapy [22,23].

The observation that PLWH who underwent ICI also show decreased survival rates might indicate that ICI does not induce as durable responses in this population as in PLw/oH, especially because time on treatment was similar between the two populations. Importantly, none of the PLWH patients in the ICI cohort received targeted therapy before ICI, which is a known factor affecting treatment response [24].

In addition to detailing the clinical characteristics of melanoma in PLWH, our study provides critical insights into how chronic HIV infection fundamentally alters the tumor immune landscape, potentially driving worsened outcomes for this population of patients. The complex landscape of immune dysfunction within the melanoma TME of PLWH is underscored by our identification of two enriched $CD8^+$ T cell subsets: $CD8^+$ $PD1^{INT}$ $LAG3^+$ and $CD8^+$ $PD1^{INT}$ $LAG3^-$.

PD1 and LAG3 are inhibitory receptors upregulated on $CD8^+$ T cells during chronic viral infections and within tumors. Although both initially serve as markers of T cell activation, sustained expression, especially in combination, drives T cell exhaustion. The similar frequencies of $CD8^+$ $PD1^{HIGH}$ T cells observed in both PLWH and PLw/oH likely reflect common chronic stimulation by tumor antigens or PD-L1 expression [25-27]. In contrast, the increased abundance of $CD8^+$ $PD1^{INT}$ $LAG3^{+/-}$ T cells in PLWH points to a population of recently activated cells. The presence of LAG3 co-expression in one of the subsets suggests that these cells are transitioning from an activated state toward exhaustion. Specifically, the $CD8^+$ $PD1^{INT}$ $LAG3^-$ population may represent an activated but pre-exhausted phenotype, with their ultimate functional fate influenced by local tumor-derived cues. Supporting this interpretation, spatial transcriptomic analysis revealed elevated *LAG3* transcription localized near tumor cells, consistent with a spatially driven gradient of exhaustion. Notably, co-expression of PD1 and LAG3 on $CD8^+$ T cells has been linked to impaired anti-tumor immunity. While dual blockade of PD1 and LAG3 has shown promise in improving progression-free survival in metastatic melanoma [28-30], clinical data on ICI efficacy in PLWH remain scarce, particularly for anti-LAG3 therapies. The dynamic interplay between LAG3 and PD1 in these subsets underscores the need for further research to determine their precise roles in tumor progression and immune escape. Understanding these interactions could inform targeted therapies to restore effective anti-tumor immunity in PLWH.

Despite HIV's well-documented impact on the $CD4^+$ T cell compartment [31,32], we observed no significant differences in total $CD4^+$ T cell counts or their subsets between cohorts, suggesting that immune dysregulation in the TME of PLWH is primarily driven by $CD8^+$ T cells. This is further supported by a decreased CD4:CD8 ratio in PLWH.

Distinct $CD8^+$ T cell subsets, combined with stable overall T cell numbers, suggest an immune landscape shaped by chronic antigen stimulation and exhaustion. However, T cell exhaustion is not the sole barrier to anti-tumor immunity in PLWH. Chronic HIV infection disrupts both adaptive T cell and innate myeloid cell compartments. We observed a significant downregulation of antigen presentation genes and a shift from classical to cross-presentation mechanisms, indicative of an immune-evasive or immunosuppressive myeloid

287 phenotype [33-35]. Multiplex immunofluorescence analysis of the myeloid compartment revealed a significantly
288 higher concentration of CD11b$^+$HLA-DR$^-$CD33$^+$ cells in melanoma tumors of PLWH. These cells, defined as
289 myeloid-derived suppressor cells (MDSCs), are a rare and potent immunosuppressive subset of immature
290 myeloid cells. In healthy individuals, MDSCs typically emerge later in cancer progression, where they are
291 well-known contributors to immune evasion and immunotherapeutic resistance [36,37]. However, PLWH exhibit
292 elevated baseline levels of circulating MDSCs, regardless of ART status, likely due to chronic low-level
293 inflammation [13,15]. The recruitment of MDSCs to the melanoma tumor site, fueled by their elevated baseline
294 levels in the peripheral circulation of PLWH, may facilitate a more rapid and aggressive trajectory of
295 melanoma progression in this population [13-15,38-40]. Our data support this hypothesis, as we observed an
296 upregulation in the expression of *CCL5* in both TUMOR and TME areas. CCL5 is primarily recognized for its
297 proinflammatory properties within the T cell compartment and its role in HIV pathogenesis, as a binding
298 partner for CCR5, a co-receptor essential for HIV entry into host cells [41-44]. However, several studies have
299 linked CCL5 to the recruitment of MDSCs, including in melanoma [45-47]. Elevated MDSC levels prior to
300 initiating immunotherapy in melanoma patients have been associated with poorer treatment response and
301 reduced overall survival, and CD11b$^+$HLA-DR$^-$CD33$^+$ cells have emerged as a predictive biomarker for
302 advanced-stage melanoma prognosis [48]. Collectively, our findings suggest that MDSCs play a central role in
303 shaping the tumor landscape of PLWH and highlight the need for further investigation into their impact on
304 CD8$^+$ T cell responses, melanoma progression, and treatment outcomes.

305 Our investigation demonstrates that, despite effective ART, HIV infection fundamentally alters
306 melanoma progression, as evidenced by heightened exhausted CD8$^+$ T cell subsets and an
307 immunosuppressive myeloid cell presence within the tumors. These immune disruptions, combined with
308 delayed healthcare responses and an increased risk for metastasis, likely contribute to the elevated mortality
309 rate observed in PLWH. Collectively, these findings underscore the urgent need for inclusive clinical trials
310 and targeted therapeutic strategies to address the unique challenges faced by PLWH and improve cancer
311 outcomes for this population.

312

313 ## Methods

314

315 *Clinical electronic record patient dataset*

316 The data used in this study were collected on 08/18/2025 from the TriNetX Research Network, which
317 provided access to electronic medical records (diagnoses, procedures, medications) from approximately
318 156,111,456 patients from 108 healthcare organizations. Patient demographics include date of birth, age,
319 sex, marital status, race, and ethnicity. Demographics are coded to HL7 version 3 administrative standards.
320 For the survival studies, the date a patient was reported as “Deceased” in the dataset was used; the cause
321 of death was not available in the dataset. The “Deceased” term in the TriNetX data model pools together
322 several different sources of mortality data: documented mortality by HCOs using ICD-10 code R99 (ill-defined

and unknown cause of mortality); if mortality is reported from HCOs via death dates of patients, this is also captured and mapped to the “Deceased” term; for the subset of patients on the TriNetX networks that have additional mortality data linked to their electronic health records (closed claims, social security master death file, private obituaries, etc.), these additional sources are also mapped to the “Deceased” term. Diagnoses and medication data in the TriNetX database are obtained from electronic health records of participating healthcare organizations. Diagnoses are recorded using the ICD-10 standardized coding system, while medication information is captured through prescription and dispensing records. These data may originate from clinical documentation, problem lists, billing records, or insurance claims and are harmonized across sites to ensure consistency.

Two cohorts of patients were retrieved with the following criteria: PLWH cohort was built selecting patients that had Malignant melanoma of skin (ICD code C43) and Human immunodeficiency virus [HIV] disease (ICD code B20, 1,019 patients were retrieved); PLw/oH cohort was built selecting patients that had C43 but not code B20 (373,121 patients were retrieved). Only patients with a cancer diagnosis between 2005 and 2025 were included. Only patients with a cancer diagnosis after HIV were included in the PLWH cohort.

The following ICD codes were used for metastatic disease: C78.7 (liver and bile duct), C79.3 (brain and meninges), C77 (lymph nodes), and C78.0 (lung). Two different analyses were performed for patients with an early occurrence of metastatic disease (from day 0 to 6 months after diagnosis) and patients with a later occurrence of metastasis (6 months from melanoma diagnosis onwards). For the “All sites” category, patients who had any of the metastatic codes C77, C78.0, C79.3, and C78.7 were included. In the dataset, medications are represented at the level of ingredients, coded to RxNorm, and organized by VA or ATC classification. For the analysis of immunotherapy characteristics and outcomes, the two cohorts were filtered to include only patients who had received any of the following FDA-approved immune checkpoint inhibitors: 1094833 (ipilimumab), 1597876 (nivolumab),1547545 (pembrolizumab), 1792776 (atezolizumab), 1919503 (durvalumab) or 2596773 (relatlimab).

Inclusion and Ethics

The retrospective study is exempt from informed consent. The data reviewed is a secondary analysis of existing data, does not involve intervention or interaction with human subjects, and is de-identified per the de-identification standard defined in Section §164.514(a) of the HIPAA Privacy Rule. The process by which the data is de-identified is attested to through formal determination by a qualified expert as defined in Section §164.514(b)(1) of the HIPAA Privacy Rule. This formal determination by a qualified expert was refreshed in December 2020.

Spatial Immune Transcriptomics

De-identified melanoma patient samples were acquired from the AIDS and Cancer Specimen Resource, the Sidney Kimmel Comprehensive Cancer Center, and NYU Grossman School of Medicine.

359 Melanoma samples from people living with HIV were retrieved first, and HIV-uninfected controls were then
360 selected to match age, sex, race and ethnicity, and nature of specimens. Five-micron sections were prepared
361 after cleaning the microtome and recovering sections in RNAse-free water. Slides were processed per
362 NanoString® protocols for nCounter RNA GeoMx experiments. Slides were baked at 60°C for 2 hours and
363 loaded onto a BOND Rx stainer (Leica). Antigen retrieval was performed with EDTA-based solution (pH 9,
364 ER2 Leica, AR9640) at 100°C for 20 minutes, followed by proteinase K (Ambion, AM2546) treatment
365 (1 µg/mL, 15 minutes, room temp). Slides were stored in PBS and incubated overnight with 200 µL of GeoMx
366 Immune Pathways Hs RNA Probes (121300201) at 37°C in a HybEZ™ oven under a Hybrislip. Post-
367 hybridization, slides underwent two washes in 50% Formamide-4XSSC at 37°C and two washes in 2XSSC
368 at room temperature, then labeled with RNA-compatible melanoma morphology markers (GeoMx Melanoma
369 Morph Kit Hs RNA). All slides were processed together but loaded onto the GeoMx instrument in batches of
370 four. Automated fluorescence imaging at 20X magnification (0.4 µm/px) was followed by ROI selection based
371 on morphology and marker expression. Three to five ROIs per sample were UV-illuminated (~1 µm²
372 resolution) to release barcodes, which were aspirated and transferred to a 96-well plate. Eluted material was
373 stored at -20°C until processing at NYUGSM. Plates were lyophilized at 65°C for 1–2 hours, rehydrated in
374 DEPC water, mixed with ICP-hyb buffer and GeoMx Hyb Code Pack_RNA probes (121300402), and
375 incubated overnight at 65°C. Hybridized samples were pooled by column and run on the nCounter MAX/Flex
376 system to generate RCC files, which were analyzed using the GeoMx Control Center.
377 Read counts were normalized to the geometric mean of five housekeeping genes (OAZ1, POLR2A,
378 RAB7A, SDHA, UBB). Normalized read counts are reported in **Table S10**. Differential expression analysis
379 (DEGs) was conducted on the normalized read counts using the DEseq2 algorithm [49] in R v4.4.2 to compare
380 the TME and TUMOR across HIV-positive and HIV-negative patients.
381
382 *Immune pathways and population analysis*
383 The MCP-counter algorithm was used to calculate the enrichment scores of tailored gene sets. [50].
384 We analyzed the dataset in two different ways: a marker-genes based analysis to detect differences in an
385 immune signaling-genes based analysis (53 genes, **Table S11**) and immune population abundances (19
386 genes, **Table S12**). A multiple Welch t-test was then performed on the population or pathway scores in HIV+
387 vs. HIV- samples. Data were represented in a bubble plot with the adjusted p-value (q-value) and Log2 fold
388 change (HIV+ vs. HIV-) for the TUMOR and TME areas (R v4.4.2; ggplot2 package).
389
390 *Multiplex Immunofluorescence (mIF)*
391 mIF staining was performed on 5 µm paraffin sections with Akoya Biosciences® Opal™ reagents on
392 a Leica BondRx autostainer, according to the manufacturer's instructions. In brief, sections were treated with
393 hydrogen peroxide to block endogenous peroxidases, followed by antigen retrieval using ER2 (Leica
394 AR9640) at 100°C. Primary and secondary antibodies were applied sequentially, with each pair followed by

395 HRP-mediated tyramide signal amplification using a unique Opal® fluorophore. After each staining round,
396 antibodies were stripped via heat retrieval, leaving the fluorophore covalently bound at the antigen site.
397 Sections were counterstained with spectral DAPI (Akoya FP1490) and mounted with ProLong Gold Antifade
398 (ThermoFisher P36935). Imaging was performed using a Leica AT2 (40X) or Akoya Vectra Polaris (20X), and
399 qptiff scans were generated with PhenoImagerHT 2.0, Phenochart 2.0, and InForm 3.0. Scans were analyzed
400 in QuPath with four ROIs per sample—two central and two peripheral—independently selected by two
401 operators using fixed-threshold detection. Averages of ROIs and operators were used as replicates. Total
402 cells were detected via QuPath's DAPI-based algorithm. T cell and myeloid infiltrates were assessed using
403 two antibody panels: Panel 1 (CD8, CD4, FoxP3, Lag3, PD1, **Table S13**) and Panel 2 (CD11b, CD33, HLA-
404 DR, CD66b, **Table S14**). CD8+ and CD4+ T cells were quantified as proportions of total cells, with PD1+,
405 LAG3+, and FOXP3+ subsets reported as percentages of each compartment. CD11b+ myeloid cells and
406 their co-expression with HLA-DR, CD33, or CD66b were quantified similarly.
407
408 *Statistical analysis*
409 Data was checked for normality (Kolmogorov-Smirnov, Shapiro-Wilk test) prior to being assigned to
410 parametric or non-parametric analyses. All the datasets analyzed in this work displayed a normal distribution.
411 To compare significant differences between two groups, we used a two-tailed t-test (parametric; Welch
412 correction was applied if variances were different between groups). A $p<0.05$ was considered significant. For
413 the immune pathways and population analysis, a multiple Welch t-test was performed with an FDR of 0.01.
414 An adjusted p-value (q-value)<0.01 was considered significant. For survival studies, a Log-rank (Mantel-Cox)
415 test was used to detect differences in survival between two populations. A $p<0.05$ was considered significant.
416 For risk Ratio assessment, risk ratios with 95% confidence intervals are calculated to compare outcomes
417 between cohorts. Risk was defined as the percentage of patients in the cohort who had the outcome in the
418 time window (Risk = Patients with Outcome/Patients in Cohort). Risk Ratio was defined as the ratio of risk
419 between cohorts (Risk Ratio = Risk for Cohort 1 / Risk for Cohort 2). Cohort balancing in TriNetX was
420 conducted using propensity score–based methods. Propensity scores were estimated via logistic regression
421 models incorporating baseline demographic and clinical covariates. Patients were matched 1:1 using greedy
422 nearest-neighbor matching without replacement, applying a caliper of 0.1 pooled standard deviations of the
423 logit of the propensity score to minimize residual confounding. In addition to matching, inverse probability of
424 treatment weighting (IPTW) was applied as a sensitivity approach, assigning weights based on the inverse
425 of the estimated propensity score to create a pseudo-population in which covariate distributions were
426 independent of exposure status. Balance across matched or weighted cohorts was evaluated by comparing
427 standardized mean differences (SMDs) for each covariate, with thresholds of <0.1 considered evidence of
428 acceptable balance. TriNetX Live was utilized to perform all the population analyses. GraphPad Prism
429 v.10.4.1 was utilized to perform all the other statistical tests.
430

References.

1. Deeks SG, Lewin SR, Havlir DV: The end of AIDS: HIV infection as a chronic disease. Lancet 382:1525-33, 2013
2. Escota GV, O'Halloran JA, Powderly WG, et al: Understanding mechanisms to promote successful aging in persons living with HIV. Int J Infect Dis 66:56-64, 2018
3. Cantero-Perez J, Grau-Exposito J, Serra-Peinado C, et al: Resident memory T cells are a cellular reservoir for HIV in the cervical mucosa. Nat Commun 10:4739, 2019
4. Murray AJ, Kwon KJ, Farber DL, et al: The Latent Reservoir for HIV-1: How Immunologic Memory and Clonal Expansion Contribute to HIV-1 Persistence. J Immunol 197:407-17, 2016
5. Cohn LB, Silva IT, Oliveira TY, et al: HIV-1 integration landscape during latent and active infection. Cell 160:420-32, 2015
6. Eyawo O, Franco-Villalobos C, Hull MW, et al: Changes in mortality rates and causes of death in a population-based cohort of persons living with and without HIV from 1996 to 2012. BMC Infect Dis 17:174, 2017
7. Yuan T, Hu Y, Zhou X, et al: Incidence and mortality of non-AIDS-defining cancers among people living with HIV: A systematic review and meta-analysis. EClinicalMedicine 52:101613, 2022
8. Coghill AE, Han X, Suneja G, et al: Advanced stage at diagnosis and elevated mortality among US patients with cancer infected with HIV in the National Cancer Data Base. Cancer 125:2868-2876, 2019
9. Coghill AE, Shiels MS, Suneja G, et al: Elevated Cancer-Specific Mortality Among HIV-Infected Patients in the United States. J Clin Oncol 33:2376-83, 2015
10. Yang ZZ, Kim HJ, Villasboas JC, et al: Expression of LAG-3 defines exhaustion of intratumoral PD-1(+) T cells and correlates with poor outcome in follicular lymphoma. Oncotarget 8:61425-61439, 2017
11. Guegan JP, Peyraud F, Dadone-Montaudie B, et al: Analysis of PD1, LAG3, TIGIT, and TIM3 expression in human lung adenocarcinoma reveals a 25-gene signature predicting immunotherapy response. Cell Rep Med 5:101831, 2024
12. Grosso JF, Goldberg MV, Getnet D, et al: Functionally distinct LAG-3 and PD-1 subsets on activated and chronically stimulated CD8 T cells. J Immunol 182:6659-69, 2009
13. Qin A, Cai W, Pan T, et al: Expansion of monocytic myeloid-derived suppressor cells dampens T cell function in HIV-1-seropositive individuals. J Virol 87:1477-90, 2013
14. Singh R, Chakraborty M, Gautam A, et al: Residual immune activation in HIV-Infected individuals expands monocytic-myeloid derived suppressor cells. Cell Immunol 362:104304, 2021
15. Bronte V, Brandau S, Chen SH, et al: Recommendations for myeloid-derived suppressor cell nomenclature and characterization standards. Nat Commun 7:12150, 2016
16. El Zarif T, Nassar AH, Adib E, et al: Safety and Activity of Immune Checkpoint Inhibitors in People Living With HIV and Cancer: A Real-World Report From the Cancer Therapy Using Checkpoint Inhibitors in People Living With HIV-International (CATCH-IT) Consortium. J Clin Oncol 41:3712-3723, 2023
17. Suneja G, Boyer M, Yehia BR, et al: Cancer Treatment in Patients With HIV Infection and Non-AIDS-Defining Cancers: A Survey of US Oncologists. J Oncol Pract 11:e380-7, 2015
18. Vora KB, Ricciuti B, Awad MM: Exclusion of patients living with HIV from cancer immune checkpoint inhibitor trials. Sci Rep 11:6637, 2021
19. Barger LN, El Naggar OS, Ha B, et al: Melanoma in people living with HIV: Immune landscape dynamics and the role of immuno- and antiviral therapies. Cancer Metastasis Rev 44:9, 2024
20. Saylor D, Dickens AM, Sacktor N, et al: HIV-associated neurocognitive disorder--pathogenesis and prospects for treatment. Nat Rev Neurol 12:234-48, 2016
21. Thompson LJ, Genovese J, Hong Z, et al: HIV-Associated Neurocognitive Disorder: A Look into Cellular and Molecular Pathology. Int J Mol Sci 25, 2024
22. Kluger HM, Chiang V, Mahajan A, et al: Long-Term Survival of Patients With Melanoma With Active Brain Metastases Treated With Pembrolizumab on a Phase II Trial. J Clin Oncol 37:52-60, 2019
23. Robert C, Carlino MS, McNeil C, et al: Seven-Year Follow-Up of the Phase III KEYNOTE-006 Study: Pembrolizumab Versus Ipilimumab in Advanced Melanoma. J Clin Oncol 41:3998-4003, 2023
24. Atkins MB, Lee SJ, Chmielowski B, et al: DREAMseq (Doublet, Randomized Evaluation in Advanced Melanoma Sequencing): A phase III trial—ECOG-ACRIN EA6134. Journal of Clinical Oncology 39:356154-356154, 2021

25. Jiang Y, Li Y, Zhu B: T-cell exhaustion in the tumor microenvironment. Cell Death Dis 6:e1792, 2015

26. Kaunitz GJ, Cottrell TR, Lilo M, et al: Melanoma subtypes demonstrate distinct PD-L1 expression profiles. Lab Invest 97:1063-1071, 2017

27. Gangaev A, Rozeman EA, Rohaan MW, et al: Differential effects of PD-1 and CTLA-4 blockade on the melanoma-reactive CD8 T cell response. Proc Natl Acad Sci U S A 118, 2021

28. Andrews LP, Butler SC, Cui J, et al: LAG-3 and PD-1 synergize on CD8(+) T cells to drive T cell exhaustion and hinder autocrine IFN-gamma-dependent anti-tumor immunity. Cell 187:4355-4372 e22, 2024

29. Tawbi HA, Schadendorf D, Lipson EJ, et al: Relatlimab and Nivolumab versus Nivolumab in Untreated Advanced Melanoma. N Engl J Med 386:24-34, 2022

30. Amaria RN, Postow M, Burton EM, et al: Neoadjuvant relatlimab and nivolumab in resectable melanoma. Nature 611:155-160, 2022

31. Okoye AA, Picker LJ: CD4(+) T-cell depletion in HIV infection: mechanisms of immunological failure. Immunol Rev 254:54-64, 2013

32. Kelley CF, Kitchen CM, Hunt PW, et al: Incomplete peripheral CD4+ cell count restoration in HIV-infected patients receiving long-term antiretroviral treatment. Clin Infect Dis 48:787-94, 2009

33. Sugita M, Brenner MB: An unstable beta 2-microglobulin: major histocompatibility complex class I heavy chain intermediate dissociates from calnexin and then is stabilized by binding peptide. J Exp Med 180:2163-71, 1994

34. Sade-Feldman M, Jiao YJ, Chen JH, et al: Resistance to checkpoint blockade therapy through inactivation of antigen presentation. Nat Commun 8:1136, 2017

35. Hildner K, Edelson BT, Purtha WE, et al: Batf3 deficiency reveals a critical role for CD8alpha+ dendritic cells in cytotoxic T cell immunity. Science 322:1097-100, 2008

36. Gabrilovich DI: Myeloid-Derived Suppressor Cells. Cancer Immunol Res 5:3-8, 2017

37. Wu Y, Yi M, Niu M, et al: Myeloid-derived suppressor cells: an emerging target for anticancer immunotherapy. Mol Cancer 21:184, 2022

38. Wang L, Zhao J, Ren JP, et al: Expansion of myeloid-derived suppressor cells promotes differentiation of regulatory T cells in HIV-1+ individuals. AIDS 30:1521-1531, 2016

39. Jordan KR, Amaria RN, Ramirez O, et al: Myeloid-derived suppressor cells are associated with disease progression and decreased overall survival in advanced-stage melanoma patients. Cancer Immunol Immunother 62:1711-22, 2013

40. Ostrand-Rosenberg S, Fenselau C: Myeloid-Derived Suppressor Cells: Immune-Suppressive Cells That Impair Antitumor Immunity and Are Sculpted by Their Environment. J Immunol 200:422-431, 2018

41. Signoret N, Pelchen-Matthews A, Mack M, et al: Endocytosis and recycling of the HIV coreceptor CCR5. J Cell Biol 151:1281-94, 2000

42. Cocchi F, DeVico AL, Garzino-Demo A, et al: Identification of RANTES, MIP-1 alpha, and MIP-1 beta as the major HIV-suppressive factors produced by CD8+ T cells. Science 270:1811-5, 1995

43. Liu X, Shah A, Gangwani MR, et al: HIV-1 Nef induces CCL5 production in astrocytes through p38-MAPK and PI3K/Akt pathway and utilizes NF-kB, CEBP and AP-1 transcription factors. Sci Rep 4:4450, 2014

44. Zeng Z, Lan T, Wei Y, et al: CCL5/CCR5 axis in human diseases and related treatments. Genes Dis 9:12-27, 2022

45. Zhang Y, Lv D, Kim HJ, et al: A novel role of hematopoietic CCL5 in promoting triple-negative mammary tumor progression by regulating generation of myeloid-derived suppressor cells. Cell Res 23:394-408, 2013

46. Jackson C, Cherry C, Bom S, et al: Distinct myeloid-derived suppressor cell populations in human glioblastoma. Science 387:eabm5214, 2025

47. Schlecker E, Stojanovic A, Eisen C, et al: Tumor-infiltrating monocytic myeloid-derived suppressor cells mediate CCR5-dependent recruitment of regulatory T cells favoring tumor growth. J Immunol 189:5602-11, 2012

48. Sade-Feldman M, Kanterman J, Klieger Y, et al: Clinical Significance of Circulating CD33+CD11b+HLA-DR- Myeloid Cells in Patients with Stage IV Melanoma Treated with Ipilimumab. Clin Cancer Res 22:5661-5672, 2016

537 49. Love MI, Huber W, Anders S: Moderated estimation of fold change and dispersion for RNA-seq
538 data with DESeq2. Genome Biol 15:550, 2014
539 50. Becht E, Giraldo NA, Lacroix L, et al: Estimating the population abundance of tissue-infiltrating
540 immune and stromal cell populations using gene expression. Genome Biology 17:218, 2016

541
542
543
544
545
546
547
548
549
550
551
552
553
554
555
556
557
558
559
560
561
562
563
564
565
566
567
568
569
570
571
572
573

Table 1. Demographics of PLWH and PLw/oH with melanoma cohorts for overall survival calculations

Demographics	PLWH - n of Patients (% of Cohort)	PLw/oH - n of Patients (% of Cohort)	P-Value	Std Diff.
Total n of patients	1,019(100%)	373,121(100%)		
Age at Index (years± SD)	58.5 ± 12.2 (100%)	62.9 ± 15.6 (100%)	< 0.0001	0.3099
Male	820(80%)	193,474(52%)	< 0.0001	0.6345
Female	182(18%)	168,820(45%)	< 0.0001	0.6166
Unknown Gender	17(2%)	10,827(3%)	0.0191	0.0826
Not Hispanic or Latino	759(74%)	257,186(69%)	0.0001	0.1236
Unknown Ethnicity	217(21%)	110,298(30%)	< 0.0001	0.1907
Hispanic or Latino	43(4%)	5,637(2%)	< 0.0001	0.1629
White	855(84%)	306,531(82%)	0.1445	0.0467
Black or African American	73(7%)	3,778(1%)	< 0.0001	0.2022
Unknown Race	70(7%)	48,014(14%)	< 0.0001	0.1150
Other Race	15(1%)	9,551(3%)	0.028	0.0775
Asian	10(1%)	3,202(1%)	0.6754	0.0127
Native Hawaiian or Other Pacific Islander	10(1%)	1,558(0%)	0.0054	0.0677
American Indian or Alaska Native	10(1%)	480(0%)	< 0.0001	0.1150

587 **Table 2. Demographics of PLWH and PLw/oH with melanoma cohorts for immunotherapy survival**
588 **calculations**
589

Demographics	PLWH - n of Patients (% of Cohort)	PLw/oH - n of Patients (% of Cohort)	P-Value	Std Diff.
Age at Index (years±SD)	62 ± 11.6 (100%)	64.4 ± 14.6 (100%)	0.2074	0.1607
Male	72 (79%)	13,750 (61%)	0.0003	0.4127
Female	17 (19%)	8,408 (37%)	0.0003	0.4184
Unknown Gender	10 (11%)	542 (2%)	< 0.0001	0.3495
Not Hispanic or Latino	74 (81%)	17,270 (76%)	0.2422	0.1282
Unknown Ethnicity	15 (16%)	4,869 (21%)	0.2493	0.1269
Hispanic or Latino	10 (11%)	561 (2%)	< 0.0001	0.345
White	79 (87%)	19,834 (87%)	0.8722	0.0167
Black or African American	10 (11%)	274 (1%)	< 0.0001	0.4176
Unknown Race	10 (11%)	1,630 (7%)	0.1606	0.1328
Other Race	10 (11%)	654 (3%)	< 0.0001	0.3233
Asian	10 (11%)	243 (1%)	< 0.0001	0.426
Native Hawaiian or Other Pacific Islander	0 (0%)	23 (0%)	0.7613	0.045
American Indian or Alaska Native	0 (0%)	42 (0%)	0.6813	0.0609
Time to treatment (days±SD)	830.105 ± 1,099.998 (100%)	492.945 ± 848.165 (100%)	0.0099	2.651
Time on treatment(days±SD)	269.269 ± 291.556 (100%)	270.601 ± 260.298 (100%)	0.9878	0.0395
Lymph Node Metastasis	49(54%)	8,172(36%)	0.0005	0.3581
Lung Metastasis	13(14%)	3,632(16%)	0.7153	0.039
Brain and Meningeal Metastasis	14(16)%	4,086(18%)	0.0813	0.179
Liver Metastasis	9(10%)	2,497(11%)	0.5385	0.0619

590
591
592

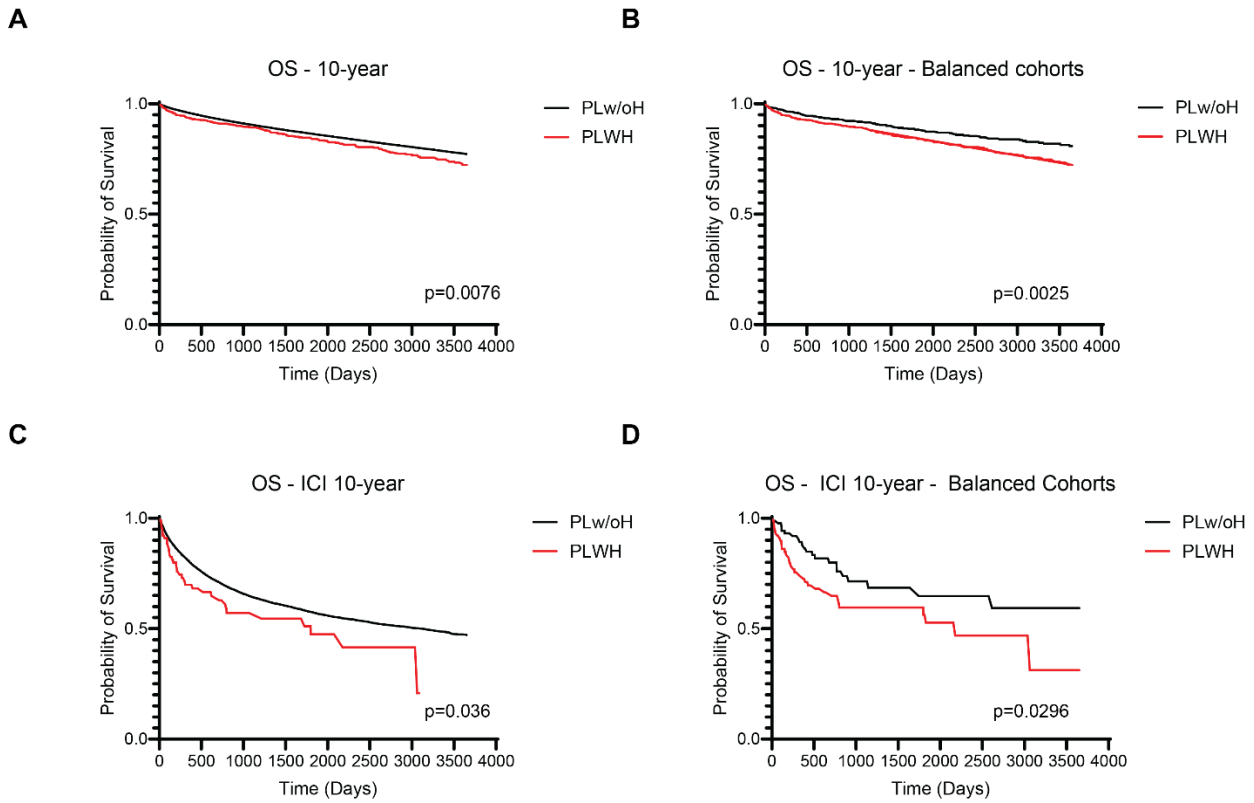

Figure 1. Overall survival rates and immune checkpoint therapy survival rates of PLWH and PLw/oH with melanoma. A-B) Kaplan-Meier graphs representing 10-year survival probability of PLWH and PLw/oH with melanoma. A) Overall survival (OS), including all patients in the cohorts. B) OS after balancing for demographics covariates. C-D) Kaplan-Meier graphs representing 10-year survival probability of PLWH and PLw/oH with melanoma who underwent immune checkpoint therapy. C) OS including all patients in the cohorts. D) OS after balancing for demographics covariates and metastasis at presentation. Reported p-values are from a Log-rank sum test between the two cohorts ($p<0.05$ is considered statistically significant).

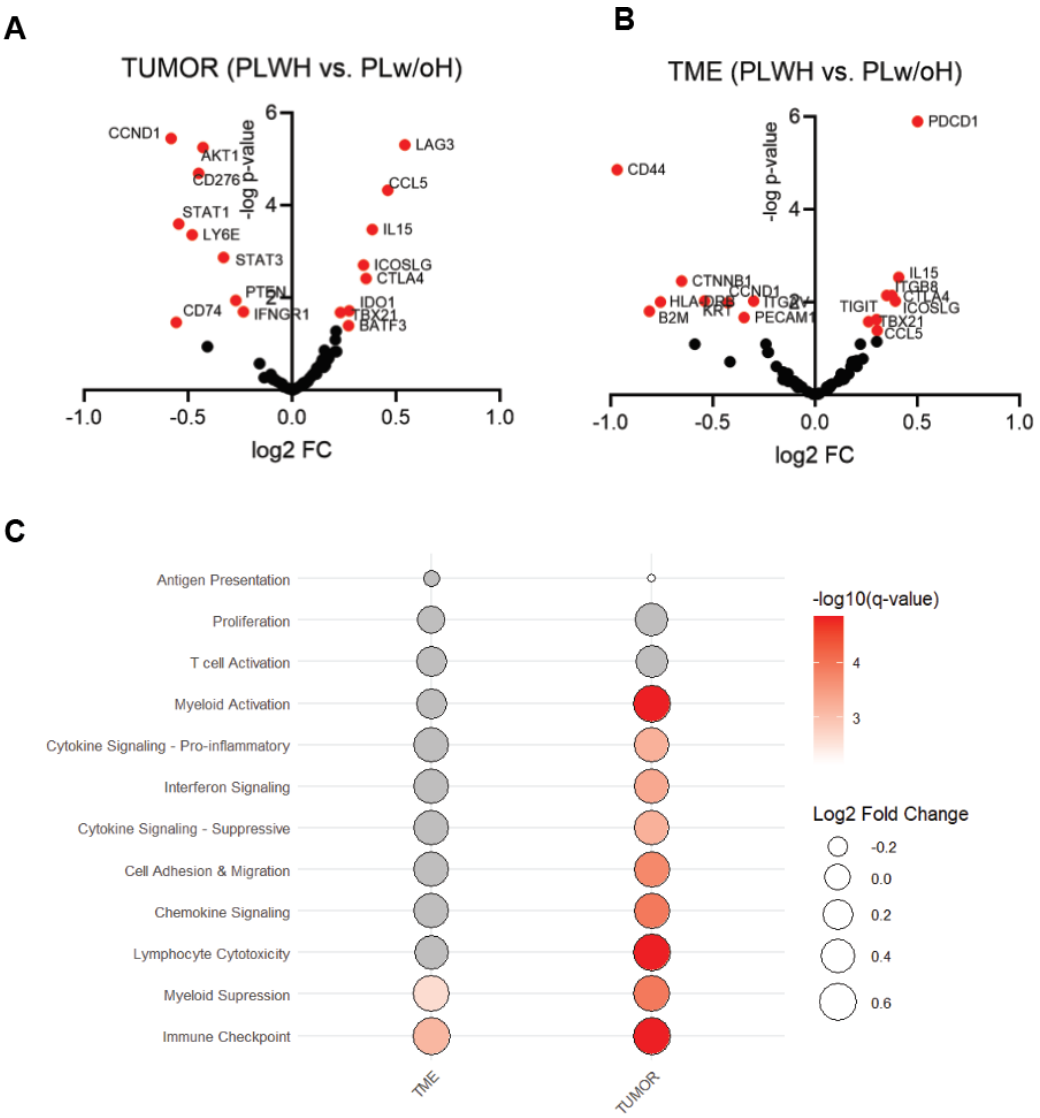

Figure 2. Spatial immune transcriptomic profiling of melanoma samples from PLWH and PLw/oH. Volcano plots for A) TME and B) TUMOR, comparing immune gene expression of PLWH vs PLw/oH melanoma samples (n=11); log2 fold change is on the x-axis, and -log10 of adjusted p-value is on the y-axis. Values were calculated by the DEseq2 algorithm (data points in red have an adjusted p-value <0.05). C) Bubble plot representation of immune signaling gene set analysis performed by running the MCPcounter algorithm on the gene expression matrix. Bubble plot size represents the log2 fold change of MCPcounter scores (PLWH vs. PLw/oH), and bubble color represents the adjusted p-value (q-value in a multiple Welch t-test with FDR of 0.01) for the TUMOR and TME areas (PLWH vs. PLw/oH). A q-value<0.01 was considered significant; comparisons with non-significant q-values are represented in grey.

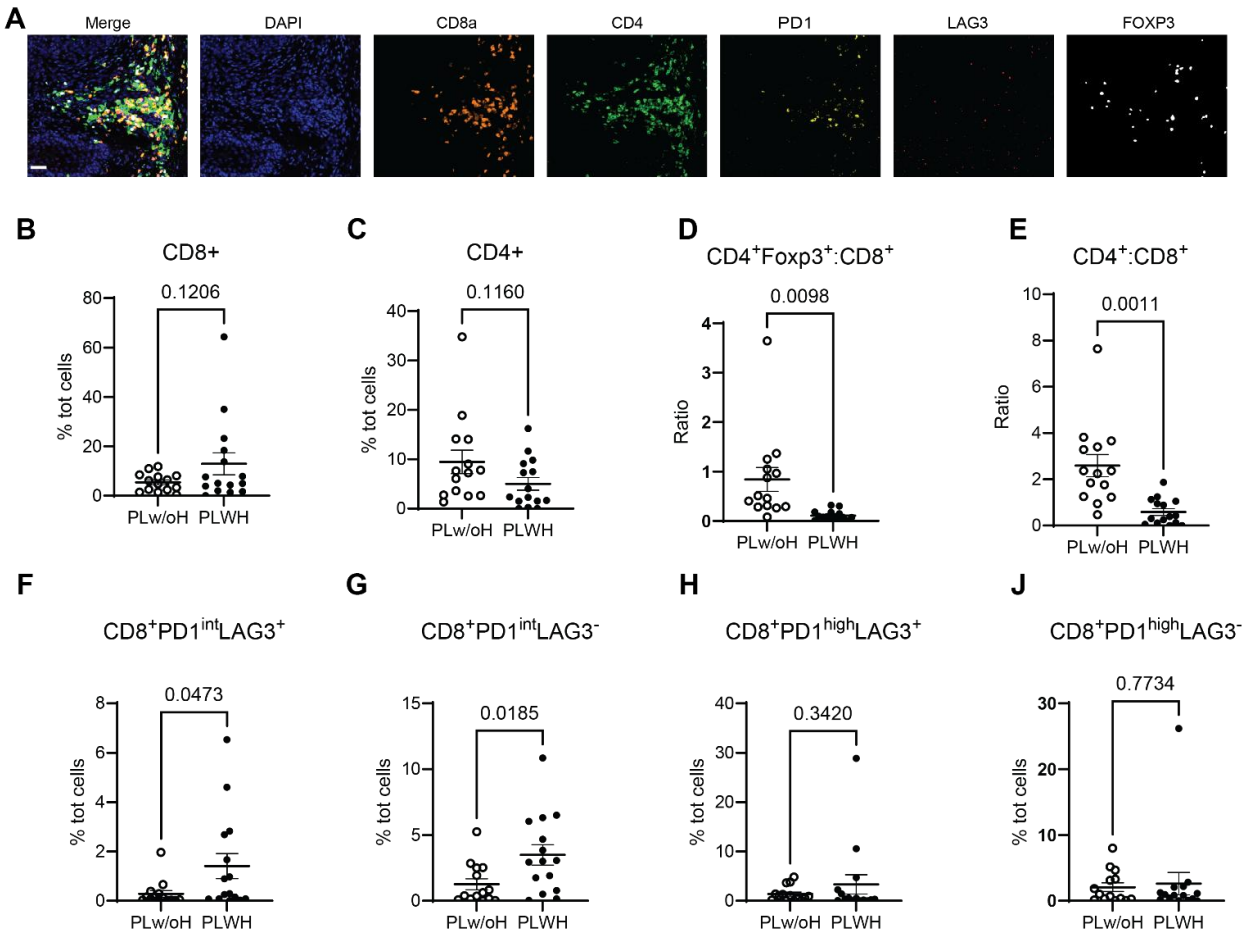

Figure 3. Multiplex IF assessment of T-cell populations' abundance and immune checkpoint expression in melanoma samples from PLWH and PLw/oH. A) Representative images of multiplex immunofluorescence (mIF) staining for the T cell panel in melanoma samples from PLWH and PLw/oH. The scale bar represents 50 µm. Quantification of mIF was performed on PLWH (n=15) and PLw/oH (n=14) tumor samples. Percentage of B) $CD8^+$ and C) $CD4^+$ T cells over the total number of cells. D) Ratio of $CD4^+Foxp3^+$ to $CD8^+$ T cells, and E) $CD4^+$ T cells to $CD8^+$ T cells. Percentage of $PD1^{int}$ $CD8^+$ T cells that are F) $LAG3^+$ and G)$LAG3^-$ over the total number of cells. Percentage of $PD1^{high}$ $CD8^+$ T-cells that are H) $LAG3^+$ and J) $LAG3^-$ over the total number of cells. The represented p-values are from a Welch's t-test; $p < 0.05$ is considered significant, and error bars represent SEM.

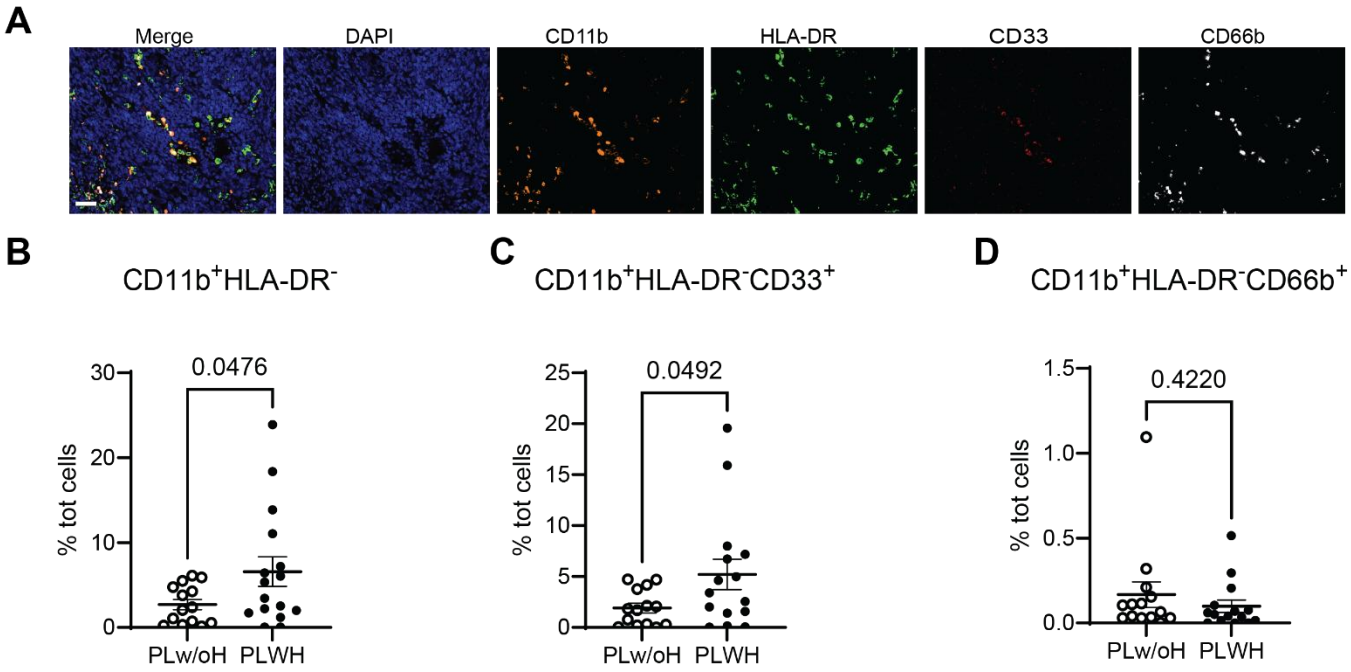

627

628 **Figure 4. Multiplex IF assessment of myeloid populations' abundance in melanoma samples from PLWH**
629 **and PLw/oH.** A) Representative images of multiplex immunofluorescence (mIF) staining for the myeloid panel
630 in melanoma samples from PLWH and PLw/oH. The scale bar represents 50 µm. Quantification of mIF was
631 performed on PLWH (n=15) and PLw/oH (n=14) tumor samples. Percentage of B) $CD11b^{+}HLA\text{-}DR^{-}$, C)
632 $CD11b^{+}HLA\text{-}DR^{-}$, $CD33^{+}$, D) $CD11b^{+}HLA\text{-}DR^{-}$, $CD66b^{+}$, over the total number of cells. The represented p-values
633 are from a Welch's t-test; $p < 0.05$ is considered significant, and error bars represent SEM.

634

635

636